

# We are IntechOpen, the world's leading publisher of Open Access books Built by scientists, for scientists

6,900

Open access books available

186,000

International authors and editors

200M

Downloads

Our authors are among the

154

Countries delivered to

TOP 1%

most cited scientists

12.2%

Contributors from top 500 universities



WEB OF SCIENCE™

Selection of our books indexed in the Book Citation Index  
in Web of Science™ Core Collection (BKCI)

Interested in publishing with us?  
Contact [book.department@intechopen.com](mailto:book.department@intechopen.com)

Numbers displayed above are based on latest data collected.  
For more information visit [www.intechopen.com](http://www.intechopen.com)



---

# Soil Moisture Retrieval from Microwave Remote Sensing Observations

---

Hongquan Wang

Additional information is available at the end of the chapter

<http://dx.doi.org/10.5772/intechopen.81476>

---

## Abstract

This chapter mainly describes the vegetated soil moisture retrieval approaches based on microwave remote sensing data. It will be comprised of three topics: (1) SAR polarimetric decomposition is to model the full coherency matrix as a summation of the surface, dihedral, and volume scattering mechanisms. After removing the volume scattering component, the soil moisture is estimated from the surface and dihedral scattering components. Particularly, various dynamic volume scattering models will be critically reviewed, allowing the readers to select the appropriate one to capture the complex variations of the volume scattering mechanism with crop phenological growth. (2) Radiative transfer model is to express the radar backscattering coefficient as the incoherent summation of different scattering components. Hereby, we will review the water cloud model and its several extensions for enhanced soil moisture retrieval. (3) Compared to the active radar, the passive radiometer possesses high temporal resolution but coarse spatial resolution. The third topic is dedicated to review the microwave emission models and the active-passive combined approaches, in the context of Soil Moisture and Ocean Salinity (SMOS) and Soil Moisture Active and Passive (SMAP) missions.

**Keywords:** soil moisture, polarimetric decomposition, radiative transfer model, microwave emission model

---

## 1. Introduction

Soil moisture is an important factor influencing the food supply to human beings at the small scale, and also an essential climate change variable that needs to be monitored at a large scale. In order to estimate the spatiotemporal dynamics of the soil moisture, the Soil Moisture and

Ocean Salinity (SMOS) satellite was launched in 2009, followed by the Soil Moisture Active and Passive (SMAP) satellite launched in 2015 although the radar component failed to send the signal back. These two missions used the microwave band, considering the dependence of the emissivity on the target dielectric constant and the penetration ability at long frequency. The microwave is found to be an appropriate frequency for monitoring the soil moisture, as it is not influenced by the cloud, and can operate day/night. Nevertheless, the passive radiometer signal is limited by the coarse spatial resolution. In contrast, the radar signal is characterized by higher spatial resolution and longer revisit time. Thus, it is appropriate to employ the radar signals for the soil moisture at a scale of agricultural fields. The polarimetric radars such as the ALOS PALSAR and RADARSAT-2 provide a full coherency or covariance matrix, which contain more information than the single-channel radar system. The PolSAR allows to extract the scattering mechanisms, which are useful for the land classification and geophysical parameter retrievals.

The soil moisture retrieval from the microwave remote sensing data is mainly influenced by the vegetation, surface roughness, and soil texture. However, over the agricultural fields, the crop characteristics vary with the phenological growth, leading to the complexity to model the vegetation influences on the soil moisture retrieval. For instance, the quality of the polarimetric soil moisture retrieval approach is highly dependent on the volume scattering model, which is used to remove the vegetation scattering contribution in the full polarized radar signal. To address this issue, several adaptive volume scattering models were developed at L-band [1] and C-band [2] for tracking the dynamic of crop growth. Both the retrieval accuracy and retrieval rate are enhanced by the dynamic volume scattering models. In contrast, in the radiative transfer models, the vegetation effect is often simulated by the vegetation optical depth, which is subsequently related to the vegetation water content and the normalized differential vegetation index (NDVI).

Within this context, this chapter provides a review of the model-based polarimetric decomposition approach, radiative transfer models, and combined active-passive methods for soil moisture retrieval over the vegetated agricultural fields. Particularly, different adaptive volume scattering models for the polarimetric decomposition are compared, and the optimal application conditions are drawn for the soil moisture retrieval. This chapter gives readers an overview of the soil moisture retrieval models at microwave band.

## **2. Soil and vegetation parameters influencing the microwave signals**

SAR system transmits polarimetric waves toward the targets and receives the backscattering signals after the interaction with ground and ground targets. This technique is of great importance for agricultural managers to monitor the soil properties and surface conditions of the agricultural fields. For example, the retrievals of soil status information from SAR can be used to identify areas at risk of erosion by water and wind. Thus, in this study, we propose to investigate soil moisture and surface roughness as two important parameters describing the

properties of bare agricultural fields. First of all, we propose to describe the parameterization of soil moisture and surface roughness.

## 2.1. Soil moisture

Soil is considered as three-phase materials: liquid phase, solid particles, and air phase. The liquid phase can be categorized into two types: the bound water and free water. Bound water is comprised of the water molecules contained in the first few molecular layers surrounding the soil particles. They are tightly held by the soil particles due to the influence of osmotic and matric forces [3, 4]. As the distance away from the soil particle surface increases, the matric forces decrease; thus the water molecules located far from the soil particle are able to move within the soil medium, which is referred as free water. Nevertheless, the criterion to separate bound water and free water is to some extent arbitrary. The amount of bound water located in the first few layers is determined by the surface area of the soil particles, which depends on the distribution of soil particle size. According to the distribution of soil particle size, different soils can be categorized into different soil textures. The solid particles are the second phase, which make up the soil skeleton. The void space between soil particles may be full of water if the soil is saturated or may be full of air if the soil is dry or may be partially saturated. The water percent hold in the soil particles is considered as soil moisture. There exist several expressions for soil moisture representation, and the frequently used approaches are the volumetric soil moisture  $mv$  and gravimetric soil moisture  $mg$ . The relationship between the volumetric soil moisture  $mv$  and gravimetric soil moisture  $mg$  is established by the water density  $\rho_w$  and total mass density  $\rho_b$ :  $mv = mg \cdot \rho_b / \rho_w$ , where  $mv$  is measured using time-domain reflectometry (TDR) and  $mg$  is used to calibrate the TDR measurements. Nevertheless, the soil texture must be taken into account in order to determine the soil capability for stocking water.

### 2.1.1. Soil texture

Soil texture is reported to have great effects on the dielectric behaviors over the entire microwave frequency range and is most significant at frequencies around 5 GHz [5]. Different soil textures can be qualitatively classified used both in field and laboratory measurements based on their physical properties. The classes are distinguished by the “textural feel” which can be further clarified by separating the relative proportions of sand, silt, and clay using grading sieves. The classes are then used to determine the crop suitability and to approximate the soil responses to environmental conditions [6]. Different soil elements which determine the specific soil texture are separated and based on the specific ranges of particle diameter  $d$  [7]:

- The smallest particles are clay particles with  $d < 0.002$  mm.
- The next smallest particles are silt particles with  $0.002 \text{ mm} < d < 0.05$  mm.
- The largest particles are sand particles with  $d > 0.05$  mm.

Soil texture classification is based on relative combination of sand, silt, and clay. Clay particles are microscopic in size and are highly plastic at moist condition. The presence of silt and/or

clay creates a fine texture soil, which impedes water and air movements. Sand-sized particles are visible with the naked eye.

### 2.1.2. Soil permittivity

The complex dielectric constant describes the behaviors of nonconductor in the electrical field. A number of factors affect the dielectric constant, such as wave frequency, temperature, and salinity of the matter. The dielectric constant represents the maximum capability to store, absorb, and conduct electric energy for a given matter. It is a measure of the medium response to the electromagnetic wave and is defined as  $\varepsilon_a = \varepsilon'_a - i\varepsilon''_a = \varepsilon_0(\varepsilon'_r - i\varepsilon''_r)$ , where  $\varepsilon_a$  represents the absolute complex permittivity,  $\varepsilon'_a$  and  $\varepsilon''_a$  are the real and imaginary parts of  $\varepsilon_a$ , and  $\varepsilon_0 = 8.85 \cdot 10^{-12}$  (F/m) is the vacuum permittivity.  $\varepsilon'_r$  is referred as the relative permittivity and considered as the dielectric constant of the specific medium.  $\varepsilon''_r$  is referred as the absorption capabilities of the medium and is relative to its conductivity and dielectric loss. For most natural medium, the condition  $\varepsilon'_r \gg \varepsilon''_r$  is satisfied.

The relative dielectric constant of water is around 80, much larger than those of solid soil (2–5) and air (around 1) [3]. Hence, the permittivity of natural soils which are mixtures of three matters is influenced largely by water content. It is viable to measure the dielectric constant in order to infer the soil water content. However, under very dry soil conditions, the real part of the dielectric constant  $\varepsilon'_r$  ranges from 2 to 4, and the imaginary part  $\varepsilon''_r$  is below 0.05 [8]. This low dielectric constant results in the soil moisture underestimation by TDR instruments, because the water is tightly bounded to the surface of soil particle, and it causes only a relatively small increase of soil permittivity which cannot be detected by TDR. On the contrary, as the water content continues to increase, above the specific transition soil moisture value (free water becomes dominant in soils), the soil permittivity will increase rapidly.

In addition, assuming the propagating wave attenuates exponentially in soils, the penetrating depths  $\delta_p$  of microwave into the soil (skin depth) can be calculated as [9, 10]

$$\delta_p = \frac{\lambda \sqrt{\varepsilon'_r}}{2\pi \varepsilon''_r} \quad (1)$$

It is noted that as the wavelength increases, the penetrating depth increases, as shown in **Figure 1** for L-, C-, and X-band, respectively. Meanwhile, for a given wavelength, the penetrating depth decreases as soil moisture increases.

### 2.1.3. Conversion between soil moisture and soil dielectric constant

*Topp model:* The soil permittivity is expressed as a three-order polynomial function in Topp model [4], which is only available for wave frequency between 20 MHz and 1 GHz:

$$\varepsilon'_r = 3.03 + 9.3mv + 146mv^2 - 76.7mv^3 \quad (2)$$

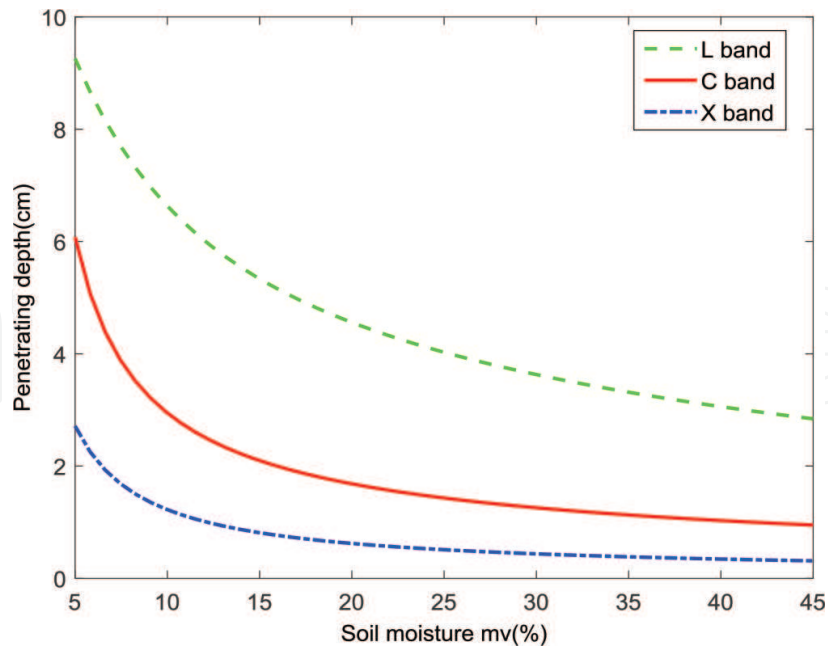


**Figure 1.** The penetrating depth in terms of radar frequency and soil moisture.

Inversely, the soil moisture is deduced from the soil permittivity measurements by a similar three-order polynomial equation:

$$mv = -5.3 \times 10^{-2} + 2.92 \times 10^{-2} \varepsilon_r' - 5.5 \times 10^{-4} \varepsilon_r'^2 + 4.3 \times 10^{-6} \varepsilon_r'^3 \quad (3)$$

This model does not consider the imaginary part of dielectric constant, and the main restriction is that the used frequency must be less than 1 GHz. The in situ soil moisture measurements using TDR are based on this model.

*Hallikainen model:* A more applicative conversion model is proposed by [5], and the soil permittivity is modeled as a function of soil moisture and soil texture in a two-order polynomial form:

$$\varepsilon_r = (a_0 + a_1S + a_2C) + (b_0 + b_1S + b_2C)mv + (c_0 + c_1S + c_2C)mv^2 \quad (4)$$

where  $a_i$ ,  $b_i$ , and  $c_i$  ( $i = 1, 2, 3$ ) are the complex coefficients for difference wave frequency between 1.4 and 18 GHz. Thus, both the real and imaginary parts of soil permittivity can be modeled. The S and C represent the percentage of silt and clay components, respectively.

*Mironov model:* The soil dielectric constant depends on the soil water content, temperature, texture, and wavelength. In the past decades, the semiempirical models in [4, 11] were mainly used for both the active and passive microwave remote sensing of soil moisture. Furthermore, Mironov dielectric model [12] considers the difference between the bound water and free water in the soil layers, which is found to be better for soil moisture retrieval at L-band.

## 2.2. Surface roughness

Besides the soil moisture, the surface roughness is another important factor that affects the backscattering SAR signature, because it determines how the incidence wave interacts with the surface. There exist several ways to describe the natural surface roughness, and two frequently used methods are mentioned here: the fractal geometry theory and the statistical description.

### 2.2.1. Fractal description

The fractal geometry theory was introduced in [13] to describe the complicated surface roughness structure, especially for the irregular and fragmented soil structures. This surface roughness description approach is proved to be suitable for natural soil because of its self-similarity, no matter what the surface scale is. In addition, many basic natural physical processes generate fractal surface; thus fractal structure is quite common in natural environment.

The fractal models describe the local structure of the soil surface using one parameter, the fractal dimension  $D$ , ranged from 1 to 2. The higher the fractal dimension, the rougher the surface. One of the frequently used fractal approaches is the Brownian model [14, 15] for a limited fractal profile. In this model, the surface profile height  $h(x)$  at location  $x$  is considered to be a fractional Brownian function: For any  $x$  and  $\Delta x > 0$ , the increase of surface height  $h(x + \Delta x) - h(x)$  follows a Gaussian distribution with mean value zero and variance  $A\Delta x^{2H}$ . Consequently, the expected value of the surface elevation increase is derived as

$$E[h(x + \Delta x) - h(x)] = 2 \int_0^{\infty} \frac{u}{\sqrt{2\pi A\Delta x^{2H}}} \exp\left(\frac{-u^2}{2A\Delta x^{2H}}\right) du = \Delta x^H E[h(x + 1) - h(x)] \quad (5)$$

where  $A$  is the variance of the normal distribution  $h(x + 1) - h(x)$  and  $H$  is the Hurst exponent constant ranged from 0 to 1. The equation is rewritten in logarithm format in order to resolve  $H$ :

$$\log [h(x + \Delta x) - h(x)] = H \log(\Delta x) + \log [h(x + 1) - h(x)] \quad (6)$$

In this equation, the parameter  $H$  equals to the slope of  $\log [h(x + \Delta x) - h(x)]$  in terms of  $\log(\Delta x)$ . It is calculated by using minimum RMSE method [16]. Consequently, the fractal dimension  $D$  can be obtained directly from  $H$  by the relationship  $D = 2 - H$ .

### 2.2.2. Statistical description

The second approach to describe the surface roughness is from the statistical point of view. There are two parameters to describe the statistical variations of the surface height relative to a reference surface: the standard deviation of the surface height  $s$  is to quantify the vertical

roughness, while the correlation length  $l$  (with autocorrelation function) is to characterize the horizontal roughness [9, 17].

Suppose a surface in the  $x$ - $y$  plane and the height of point  $(x, y)$  are assumed to be  $z(x, y)$  above the  $x$ - $y$  plane. A representative surface with dimensions  $L_x$  and  $L_y$  is segmented statistically, which is centered at the original point.

The average height of the surface is given by

$$\bar{z} = \frac{1}{L_x L_y} \int_{-L_x/2}^{L_x/2} \int_{-L_y/2}^{L_y/2} z(x, y) dx dy \quad (7)$$

and the second moment is given by

$$\bar{z}^2 = \frac{1}{L_x L_y} \int_{-L_x/2}^{L_x/2} \int_{-L_y/2}^{L_y/2} z^2(x, y) dx dy \quad (8)$$

Consequently, the standard deviation of the surface height within the area  $L_x \times L_y$  is defined as

$$s = \sqrt{\overline{z^2} - \bar{z}^2} \quad (9)$$

The formulation above can be reduced to a discrete condition. The surface profiles are digitized into discrete values  $z_i(x_i)$  at spacing rate  $\Delta x$  which is satisfied the criterion  $\Delta x < 0.1\lambda$  as described in [3]. The standard deviation  $s$  for discrete condition is formulated as

$$s = \sqrt{\frac{\sum_{i=1}^N (z_i)^2 - N(\hat{z})^2}{N - 1}} \quad (10)$$

where  $\hat{z} = \frac{\sum_{i=1}^N z_i}{N}$  is the mean surface height and  $N$  is the number of samples.

For the horizontal surface roughness description, the surface autocorrelation function (ACF) has to be determined. The autocorrelation function  $\rho$  characterizes the independence of two points at a distance  $\sqrt{\xi^2 + \zeta^2}$ :

$$\rho(\xi, \zeta) = \frac{\int_{-L_x/2}^{L_x/2} \int_{-L_y/2}^{L_y/2} z(x, y) z(x + \xi, y + \zeta) dx dy}{\int_{-L_x/2}^{L_x/2} \int_{-L_y/2}^{L_y/2} z^2(x, y) dx dy} \quad (11)$$

In the discrete case, the autocorrelation function for a spatial displacement  $x_i = (j - 1)\Delta x$  is defined as

$$\rho(\xi) = \frac{\sum_{i=1}^{N+1-j} z_j z_{j+i-1}}{\sum_{i=1}^N z_i^2} \quad (12)$$

where  $z_{j+i-1}$  is a point with the spatial displacement  $x_i$  from the point  $z_i$ . The surface correlation length  $l$  is then defined as the displacement  $x_i$ , under which the  $\rho(x_i)$  between the two points equals  $1/e$ . The correlation length characterizes the statistical independence of two points. In case that the distance between two points is larger than  $l$ , their heights can be considered statistically independent from each other. For very smooth surface, the correlation length is toward infinity.

### 2.2.3. Wave interaction with the surface roughness

Furthermore, the effective surface roughness observed by SAR system depends on microwave wavelength. For instance, a given surface that appears smooth in L-band may seem rough in C-band. The relative surface roughness status (compared with wavelength) affects the surface scattering behaviors:

- For the smooth surface, the angular radiation pattern of the reflected wave is modeled as a delta function which is centered about the specular direction.
- For the medium roughness surface, the angular radiation pattern is comprised of coherent component and incoherent component. The coherent component is radiated in the specular direction even though its magnitude is smaller than over the smooth surface. The incoherent scattering component consists of energy scattered in all directions, but its magnitude is smaller than that of the coherent component.
- For the rough surface, the radiation pattern seems like a Lambertian surface, comprised of only incoherent scattering.

Thus, in the electromagnetic models, the effective vertical and horizontal surface roughness is given in terms of the production with EM wave number ( $k = 2\pi f/c$ ):  $ks$  and  $kl$ . It is obvious that  $ks$  and  $kl$  are decreasing with increasing wavelength. Consequently, as shown in **Figure 2**, the surface roughness is one of the important factors that determine the electromagnetic wave response from bare soil.

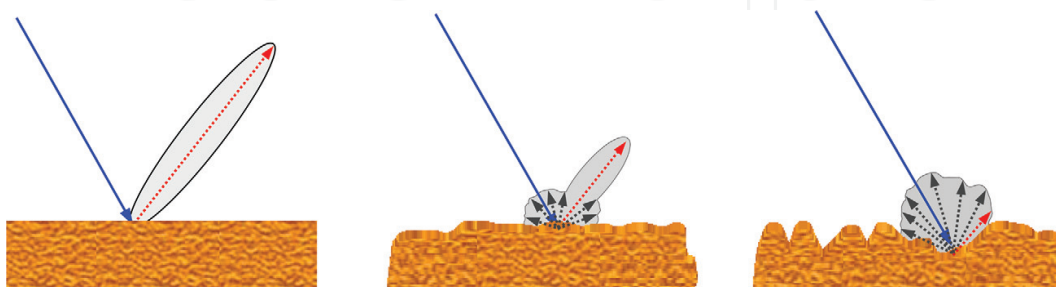


**Figure 2.** Scattering patterns determined by surface roughness.

#### 2.2.4. Bragg phenomenon

Except the surface roughness and soil moisture, the row direction also influences the backscattering SAR wave from the bare agricultural soils, because it induces the Bragg phenomenon. Bragg resonance is a type of coherent scattering, which is present in some agricultural fields due to the plowing or other row structures' tillage. The resonance occurs in case that the distance between radar and each of the periodic structures has an additional phase difference of  $\lambda/2$  in the slant-range direction. Under this condition, the additional phase shift is  $2\pi$ , and the signals will add in phase.

#### 2.3. Vegetation

Vegetation has two effects on the radar signal: (1) attenuate the backscattering from the underlying soils and (2) produce the volume scattering adding to the radar signal. These two effects increase the complexity of soil moisture retrieval from microwave signal. The vegetation attenuation and scattering effects were parameterized by the vegetation scattering albedo and optical depth, which are related to the vegetation water content or leaf area index.

A. Vegetation optical depth  $\tau$  is linked to the vegetation water content through  $b$  parameter:

$$\tau = bVWC \quad (13)$$

The  $b$  parameter depends on the crop type, structure, and growth stage and microwave polarization. The vegetation water content is often obtained from the NDVI. Alternatively,  $\tau$  can be obtained from the LAI through a linear relationship:

$$\tau = b_1LAI + b_2 \quad (14)$$

The  $b_1$  and  $b_2$  are assumed to be dependent on the vegetation type.

B. Vegetation scattering albedo  $\omega$  is set to be zero or a low value in the passive radiometer analysis.

### 3. Polarimetric decomposition for soil moisture estimation

Depending whether the sensor generates the microwave by itself, the microwave remote sensing can be categorized into the active and passive, which are reviewed separately. Polarimetric SAR is a coherent active microwave remote sensing system, providing backscattering signals in quad-polarization states with fine spatial resolution. Unlike the optical remote sensing, the SAR system monitors the earth using a side-look geometry, resulting in the issues of overlap, shadow, and forth short. Furthermore, at the microwave bands, the signals are sensitive to the permittivity and the structure of the targets. Thus, the interpretation and modeling of the SAR data differ from those of optical domain. The SAR system generates the microwave, so that it operates regardless the light and day/night and clear/cloudy conditions.

This is particularly interesting for monitoring the soil moisture over the area frequently covered by the cloud.

### 3.1. Decomposition theories

#### 3.1.1. Polarimetric SAR data expression

The microwave scattering process over the ground can be formulated  $E_S = [S]E_I$ , where the Sinclair matrix  $[S]$  relates the incident wave  $E_I$  to the scattering wave  $E_S$ . Thus, the polarimetric SAR data extracted as  $[S]$  includes the target dielectric and structural properties:

$$[S] = \begin{bmatrix} S_{HH} & S_{HV} \\ S_{VH} & S_{VV} \end{bmatrix} \quad (15)$$

where  $S_{HH}$  and  $S_{VV}$  are the co-polarized scatterings, and  $S_{HV}$  and  $S_{VH}$  represent the cross-polarized scattering power. They are all complex numbers. For the monostatic case of back-scattering, the satisfied reciprocity results in  $S_{HV} = S_{VH}$ . This format of  $[S]$  matrix is considered as single-look data suffering from the speckle effect, as no averaging process is performed.

However, the natural targets dynamically vary with time, requiring a statistical description such as the second-order moment approach. In order to extract more polarimetric information such as the correlation between different polarimetric channels, the Pauli and Lexicographic vectors are constructed from the  $[S]$  matrix, respectively:

$$k = [S_{HH} + S_{VV}, S_{HH} - S_{VV}, 2S_{HV}]^T \quad (16)$$

$$\Omega = [S_{HH}, \sqrt{2}S_{HV}, S_{VV}]^T \quad (17)$$

From the Pauli and Lexicographic vectors, the coherency matrix  $[T]$  and the covariance matrix  $[C]$  are obtained by  $[T] = \langle k \cdot k^{*T} \rangle$  and  $[C] = \langle \Omega \cdot \Omega^{*T} \rangle$ , where the symbol  $\langle \rangle$  means the temporal or spatial averaging to reduce the randomness of the polarimetric images. In the monostatic condition (transmitter and receiver in the same location), they are expressed as

$$[T3] = \begin{bmatrix} T_{11} & T_{12} & T_{13} \\ T_{12}^* & T_{22} & T_{23} \\ T_{13}^* & T_{23}^* & T_{33} \end{bmatrix} = 0.5 \begin{bmatrix} \langle |S_{HH} + S_{VV}|^2 \rangle & \langle (S_{HH} + S_{VV})(S_{HH} - S_{VV})^* \rangle & 2\langle (S_{HH} + S_{VV})S_{HV}^* \rangle \\ \langle (S_{HH} + S_{VV})^*(S_{HH} - S_{VV}) \rangle & \langle |S_{HH} - S_{VV}|^2 \rangle & 2\langle (S_{HH} - S_{VV})S_{HV}^* \rangle \\ 2\langle (S_{HH} + S_{VV})^*S_{HV} \rangle & 2\langle (S_{HH} - S_{VV})^*S_{HV} \rangle & 4\langle |S_{HV}|^2 \rangle \end{bmatrix} \quad (18)$$

$$[C3] = \begin{bmatrix} C_{11} & C_{12} & C_{13} \\ C_{12}^* & C_{22} & C_{23} \\ C_{13}^* & C_{23}^* & C_{33} \end{bmatrix} = \begin{bmatrix} \langle |S_{HH}|^2 \rangle & \sqrt{2}\langle S_{HH}S_{HV}^* \rangle & \langle S_{HH}S_{VV}^* \rangle \\ \sqrt{2}\langle S_{HH}^*S_{HV} \rangle & 2\langle |S_{HV}|^2 \rangle & \sqrt{2}\langle S_{HV}S_{VV}^* \rangle \\ \langle S_{HH}^*S_{VV} \rangle & \sqrt{2}\langle S_{HV}^*S_{VV} \rangle & \langle |S_{VV}|^2 \rangle \end{bmatrix}$$

The polarimetric decompositions are often done on the coherency matrix [T3] and the covariance matrix [C3], which can be converted between each other via unitary transformation. However, the elements of the [T3] matrix are physically convenient. For instance, the  $T_{11}$ ,  $T_{22}$ , and  $T_{33}$  can be used to approximate the surface, dihedral, and volume scattering powers.

### 3.1.2. Eigen-based decomposition

Both [T3] and [C3] matrices are characterized by nonnegative eigenvalues and orthogonal eigenvector. The classical decomposition approach proposed by Cloude and Pottier relies on the eigenanalysis on the [T3] matrix. The scattering mechanism and the corresponding relative power were quantified by the eigenvector ( $T_i$ ) and eigenvalues ( $\lambda_i$ ), respectively:

$$[T3] = \lambda_1 T_1 + \lambda_2 T_2 + \lambda_3 T_3 \quad (19)$$

From the eigenvalues and eigenvectors, the entropy  $H$  and  $\alpha$  angle are defined to characterize the randomness of the scattering scene and the dominant scattering mechanism:

$$H = \sum_{i=1}^3 -p_i \log_3 p_i \quad \alpha = \sum_{i=1}^3 p_i \arccos(|e_{i1}|) \quad \text{and} \quad p_i = \lambda_i / \sum_{i=1}^3 \lambda_i \quad (20)$$

In addition, the scattering anisotropy  $A$  is introduced to discriminate the ambiguous case of  $H > 0.7$ :

$$A = (\lambda_2 - \lambda_3) / (\lambda_2 + \lambda_3) \quad (21)$$

These polarimetric parameters are used to describe the scattering mechanisms under a variety of scenarios. However, in Baghdadi et al. [18], the sensitivity of entropy and  $\alpha$  angle to soil moisture and surface roughness is analyzed, indicating insignificant response of these polarimetric parameters to the soil characteristics at C-band.

### 3.1.3. Model-based decomposition

Under the assumption of reflection symmetry (zero correlation between the co- and cross-polarization channels), the Freeman-Durden decomposition models the covariance matrix [C3] as the incoherent summation of the surface, dihedral, and volume scattering components.

In order to be consistent with previous eigen-based approach, we express the Freeman-Durden decomposition based on [T3] matrix [19]:

$$[T3] = \begin{bmatrix} T_{11} & T_{12} & 0 \\ T_{12}^* & T_{22} & 0 \\ 0 & 0 & T_{33} \end{bmatrix} = f_s \begin{bmatrix} 1 & \beta^* & 0 \\ \beta & |\beta|^2 & 0 \\ 0 & 0 & 0 \end{bmatrix} + f_d \begin{bmatrix} |\alpha|^2 & \alpha & 0 \\ \alpha^* & 1 & 0 \\ 0 & 0 & 0 \end{bmatrix} + f_v \begin{bmatrix} V_{11} & 0 & 0 \\ 0 & V_{22} & 0 \\ 0 & 0 & V_{33} \end{bmatrix} \quad (22)$$

The surface component is modeled using the simple Bragg model. The polarimetric parameter  $\beta = \frac{R_H - R_V}{R_H + R_V}$  and  $f_s = 0.5|R_H + R_V|^2$  are constructed from the Bragg scattering coefficients:

$$R_H = \frac{\cos \theta - \sqrt{\varepsilon - \sin^2 \theta}}{\cos \theta + \sqrt{\varepsilon - \sin^2 \theta}}, R_V = \frac{(\varepsilon - 1)(\sin^2 \theta - \varepsilon(1 + \sin^2 \theta))}{(\varepsilon \cos \theta + \sqrt{\varepsilon - \sin^2 \theta})^2} \quad (23)$$

The dihedral component is developed from the Fresnel coefficients of the orthogonal dielectric planes between the plant stalks and the underlying soils. The scattering amplitude  $f_d = 0.5|R_{SH}R_{TH} + R_{SV}R_{TV}e^{i\psi}|^2$  and polarization ratio  $a = \frac{R_{SH}R_{TH} - R_{SV}R_{TV}e^{i\psi}}{R_{SH}R_{TH} + R_{SV}R_{TV}e^{i\psi}}$  are related to the Fresnel coefficients of soil and plant:

$$R_{jH} = \frac{\cos \theta_j - \sqrt{\varepsilon_i - \sin^2 \theta_j}}{\cos \theta_j + \sqrt{\varepsilon_i - \sin^2 \theta_j}} \text{ and } R_{jV} = \frac{\varepsilon_i \cos \theta_j - \sqrt{\varepsilon_i - \sin^2 \theta_j}}{\varepsilon_i \cos \theta_j + \sqrt{\varepsilon_i - \sin^2 \theta_j}} \quad (24)$$

where  $j$  represents soil (S) or plant (T). In the dihedral geometric configuration, the incidence angle over soil  $\theta_S$  and over the plant  $\theta_T$  is supplementary ( $\theta_S + \theta_T = \frac{\pi}{2}$ ).

The vegetation volume is simulated by the dipole with a uniform statistical distribution. Consequently, the volume component is derived as

$$[V] = f_v \begin{bmatrix} 0.5 & 0 & 0 \\ 0 & 0.25 & 0 \\ 0 & 0 & 0.25 \end{bmatrix} \quad (25)$$

The Freeman-Durden model is firstly fitted to the forest scenario, and it is reported to be effective to discriminate the forest and deforest areas.

## 3.2. Soil moisture retrieval using polarimetric decomposition techniques

### 3.2.1. Model-based decomposition

The polarimetric soil moisture retrieval can be conducted based on the model-based decomposition, in which the soil dielectric constant is related to the surface scattering component through the Bragg scattering model and to the dihedral component through the combined Fresnel scattering model. Nevertheless, in the past decades, the model-based polarimetric

decompositions were mainly applied to the image classification, target detection by analyzing the scattering mechanisms. Hajnsek et al. [19] proposed to estimate the soil moisture from the L-band polarimetric decomposition. In their approach, after removing the volume component from the full signature, the soil moisture is retrieved from the surface and dihedral scattering component, respectively.

For the surface scattering component, the polarimetric parameter  $\beta$  is related to the soil moisture and incidence angle (Figure 3). Unlike the traditional radar backscattering coefficients which are more sensitive to soil moisture at low incidence angle condition, the polarimetric parameter  $\beta$  is more sensitive to the soil moisture at high incidence angle. Thus, depending on the incidence angle ranges of the radar data, the traditional direct backscattering approach or the advanced polarimetric approach is preferable. In Hajnsek et al. [19], the surface scattering component is adapted by replacing the Bragg model with the X-Bragg model in order to take the surface roughness effect into account.

In contrary to the surface scattering component, the dihedral scattering component is influenced by both the soil and vegetation dielectric constants. Thus, two equations were required to decouple the soil and vegetation contributions on the dihedral component, in order to extract the soil moisture from it. In the literature [19, 20], the parameter  $\alpha$  and  $f_d$  are used to construct an equation system, from which the soil and vegetation dielectric constants are solved. Nevertheless, the vegetation dielectric constant is not furthermore considered, as the main purpose of this chapter is to estimate the soil moisture from microwave remote sensing data.

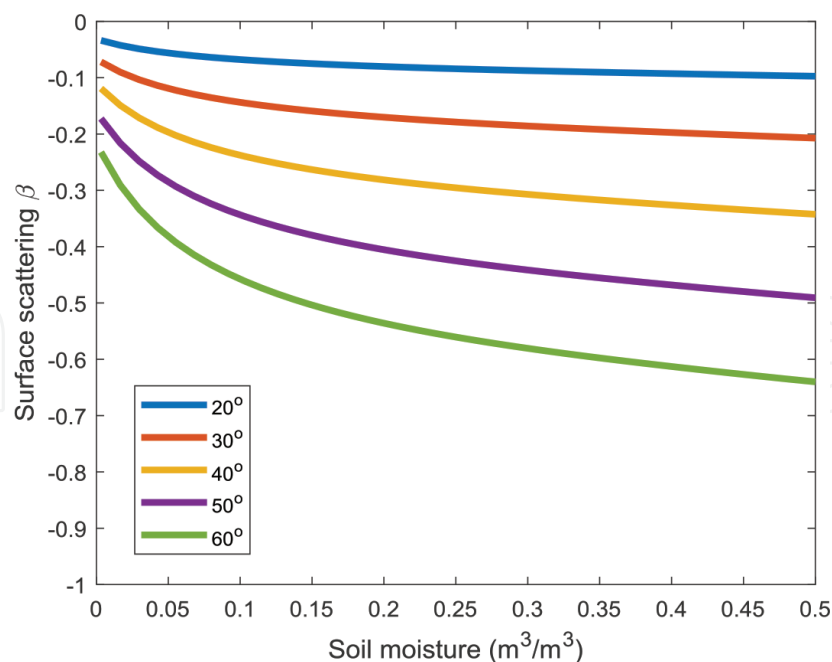


Figure 3. Sensitivity of surface scattering parameter  $\beta$  to soil moisture.

Figures 4, 5 plot the  $\alpha$  and  $f_d$  in terms of soil and vegetation dielectric constants:

- Parameter  $\alpha$  is more sensitive to soil moisture when the incidence angle is less than  $45^\circ$ ; otherwise, it is more sensitive to vegetation dielectric constants.
- For the  $f_d$  parameter, the sensitivity to soil moisture is the same between the low and high incidence angles, while the absolute value of  $f_d$  is different.

The dihedral scattering component is complementary to the surface component, increasing the overall retrieval rate. The surface scattering component which is the function of only soil dielectric constant is generally easier for the soil moisture retrieval than the dihedral component which is the function of both soil and vegetation dielectric constants. However, for some crop types such as canola and wheat, the significant dihedral scattering power at the early phenological stages contributes largely to the soil moisture [21]. There is a limitation in the dihedral component at incidence angle around  $45^\circ$ , when the soil and vegetation dielectric constants are not possible to be decoupled from each other.

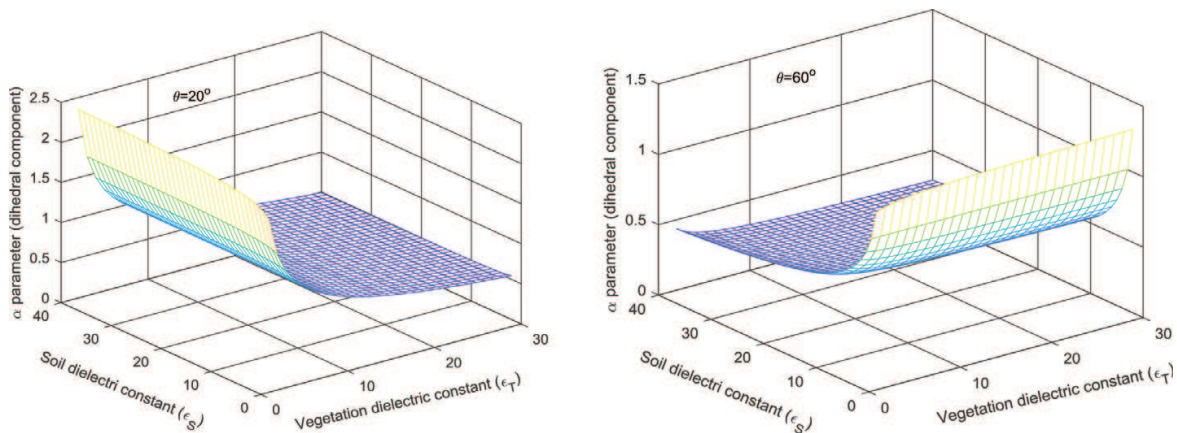


Figure 4. Sensitivity of dihedral parameter alpha to soil and vegetation dielectric constants under low and high incidence angles.

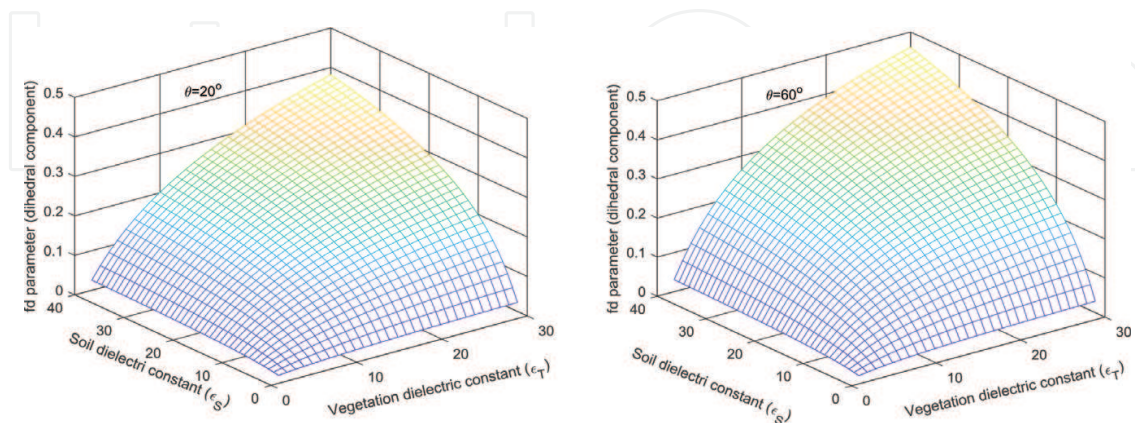


Figure 5. Sensitivity of alpha parameter  $f_d$  to soil and vegetation dielectric constants under low and high incidence angles.

It is in the consensus that the most challenging issue is the modeling of the volume scattering component. With the crop growth, the shape and crop structures vary dynamically, which makes the unique volume coherency matrix fail to capture the high complexity of the crop growth. In order to analyze this issue, Hajnsek et al. [19] compared several volume scattering formulations. One is the flexible volume model in Yamaguchi et al. [22], where the crops are described in vertical, random, and horizontal orientations. The volume coherency matrix was derived considering the dipoles with different orientation angle distribution widths. The parameter  $Pr = 10 \log_{10}(VV)/10 \log_{10}(HH)$  is used to determine the dominant orientation:

$$T_V = \frac{fv}{30} \begin{bmatrix} 15 & 5 & 0 \\ 5 & 7 & 0 \\ 0 & 0 & 8 \end{bmatrix}, T_R = fv \begin{bmatrix} 0.5 & 0 & 0 \\ 0 & 0.25 & 0 \\ 0 & 0 & 0.25 \end{bmatrix}, T_H = \frac{fv}{30} \begin{bmatrix} 15 & -5 & 0 \\ -5 & 7 & 0 \\ 0 & 0 & 8 \end{bmatrix} \quad (26)$$

Another volume coherency matrix is proposed by narrowing the dipole orientation angle around radar line of sight. However, for all the volume models in [19], the corresponding soil moisture retrieval results indicate an underestimation for the wheat and corn fields, while an over-/underestimation for the rape fields. So far, there is no universal volume coherency matrix which performs well for all the crop types and the whole phenological development stages.

Furthermore, Jagdhuber et al. [20] developed an L-band polarimetric decomposition for the multiangular soil moisture retrieval over the agricultural fields covered by low vegetation. In the study, the multiangular observation was conducted by three flight lines over the same area. The effects of microwave extinction and phase shift on the surface and dihedral scattering component were accounted. For each pixel, multiple  $\beta$ ,  $\alpha$ , and  $fd$  were obtained for a joint retrieval process. The soil moisture retrieval obtained an RMSE ranging from 0.06 to 0.08 m<sup>3</sup>/m<sup>3</sup>.

Recently, the hybrid decomposition which combines the model-based and eigen-based decompositions is used for the soil moisture retrieval [1]. After extracting the volume scattering component using the model-based approach, the remaining ground scattering component is decomposed again using the eigen-based approach in order to better discriminate the surface and dihedral scattering mechanisms, taking advantages of the orthogonality of the eigenvector. This avoids the assumption of the dominant scattering mechanism in the ground component, in the original Freeman-Durden decomposition approach [23].

In addition, the deorientation process is accounted before conducting the polarimetric decomposition, to reduce the fluctuation due to the random orientation angle of each pixel. This was done by minimizing the cross-polarization power [24]. After the deorientation process, the pixel with different orientation angles will result in the same decomposition results. Wang et al. [25] studied effectivity of the deorientation on the polarimetric soil moisture, indicating that the surface scattering component is significantly enhanced, as a result of the deorientation process. The increase in the surface scattering power is assumed to benefit the soil moisture retrieval. This is understandable, as the surface component is a function of the soil characteristics, while the dihedral component is complicated due to the coupling between the soil and

vegetation dielectric constants. Three different polarimetric decompositions (Freeman-Durden, Hajnsek, and An) were compared for the soil moisture retrieval. However, the performances depend on the crop types and phenological stages, and none of them can perform well for all the crop types and the whole growth stages. The Hajnsek decomposition is better for the early growth stage, while the An decomposition is overperformed for the crop's later development season. The Freeman decomposition obtained better results on the corn fields with sparse planting density. Furthermore, the incidence angle normalization is conducted on the polarimetric parameters ( $\beta$ ,  $\alpha$ , and  $fd$ ) to reduce the incidence angle effect on the soil moisture retrieval.

Similar to the idea of X-Bragg model which rotates the Bragg surface around radar line of sight, the extended Fresnel model was developed for the dihedral scattering component [26]. It is achieved by rotating the soil plane of the dihedral component around the radar line of sight, to introduce the surface roughness effect on the dihedral component. Unlike the introduction of the surface roughness in the dihedral component in Hajnsek et al. [19], which did not change the matrix rank, the dihedral coherency matrix obtained in the extended Fresnel model increases the matrix rank from 1 to 3. Thus, both the amplitude and phase of the dihedral component have been changed.

### 3.2.2. Eigen-based decomposition

The eigenvalues and eigenvectors of [T] matrix were computed to construct the polarimetric parameters for characterization of the scattering mechanisms. However, the currently eigen-based decomposition is mainly limited for soil moisture retrieval over the bare soils. The first one is the X-Bragg model [27], introducing the surface roughness effect into the Bragg model by rotating the soil plane around the radar light of sight. In order to estimate the soil moisture, the X-Bragg model relates the entropy  $H$  and  $\alpha$  angle to the soil dielectric constant. A lookup table is established to determine the soil dielectric constant from the data-derived entropy and  $\alpha$  angle. In addition, the surface roughness is derived from the polarimetric anisotropy parameter.

Furthermore, under the assumption of the reflection symmetry, the polarimetric parameters which are dominated by only the soil moisture or the surface roughness were constructed from the eigenvalue and eigenvector of the coherency matrix. According to Allain [28], the analytical eigenvalues is derived as

$$\begin{aligned}\lambda_{1nos} &= 0.5 \left( \langle |S_{HH}|^2 \rangle + \langle |S_{VV}|^2 \rangle + \sqrt{\left( \langle |S_{HH}|^2 \rangle - \langle |S_{VV}|^2 \rangle \right)^2 + 4 \langle |S_{HH}S_{VV}^*|^2 \rangle} \right) \\ \lambda_{2nos} &= 0.5 \left( \langle |S_{HH}|^2 \rangle + \langle |S_{VV}|^2 \rangle - \sqrt{\left( \langle |S_{HH}|^2 \rangle - \langle |S_{VV}|^2 \rangle \right)^2 + 4 \langle |S_{HH}S_{VV}^*|^2 \rangle} \right) \\ \lambda_{3nos} &= 2 \langle |S_{HV}|^2 \rangle\end{aligned}\tag{27}$$

where the sign *nos* denotes no order in size. The corresponding analytical eigenvectors can be derived as

$$\begin{aligned}
 e_1 &= \frac{1}{\sqrt{2 \left[ \left( |S_{HH}|^2 - |S_{VV}|^2 + \sqrt{\Delta} \right)^2 + 4 |S_{HH} S_{VV}^*|^2 \right]}} \begin{bmatrix} 2S_{HH} S_{VV}^* + \left( |S_{HH}|^2 - |S_{VV}|^2 + \sqrt{\Delta} \right) \\ 2S_{HH} S_{VV}^* - \left( |S_{HH}|^2 - |S_{VV}|^2 + \sqrt{\Delta} \right) \\ 0 \end{bmatrix} \\
 e_2 &= \frac{1}{\sqrt{2 \left[ \left( |S_{HH}|^2 - |S_{VV}|^2 - \sqrt{\Delta} \right)^2 + 4 |S_{HH} S_{VV}^*|^2 \right]}} \begin{bmatrix} 2S_{HH} S_{VV}^* + \left( |S_{HH}|^2 - |S_{VV}|^2 - \sqrt{\Delta} \right) \\ 2S_{HH} S_{VV}^* - \left( |S_{HH}|^2 - |S_{VV}|^2 - \sqrt{\Delta} \right) \\ 0 \end{bmatrix} \\
 e_3 &= \begin{bmatrix} 0 \\ 0 \\ 1 \end{bmatrix}
 \end{aligned}
 \tag{28}$$

with  $\Delta = \left( |S_{HH}|^2 - |S_{VV}|^2 \right)^2 + 4 |S_{HH} S_{VV}^*|^2$ . Based on the eigenvalues in reflection symmetry conditions, three polarimetries SERD, DERD, and SDERD are defined to characterize the difference among three scattering mechanisms (single bounce, double bounce, and multiple scattering):

$$\begin{aligned}
 \text{SERD} &= \frac{\lambda_s - \lambda_m}{\lambda_s + \lambda_m} \\
 \text{DERD} &= \frac{\lambda_d - \lambda_m}{\lambda_d + \lambda_m} \\
 \text{SDERD} &= \frac{\lambda_s - \lambda_d}{\lambda_s + \lambda_d}
 \end{aligned}
 \tag{29}$$

where  $\lambda_s = \lambda_{1nos}$  and  $\lambda_s = \lambda_{2nos}$  if  $a_1 < a_2$ . In contrary,  $\lambda_s = \lambda_{2nos}$  and  $\lambda_s = \lambda_{1nos}$  if  $a_1 > a_2$ . The  $\lambda_m = \lambda_{3nos}$  holds on in all cases. It is reported [10] that SERD is suitable to characterize vegetation, while DERD is appropriate to quantify the surface roughness. SDERD can be applied to discriminate between bare and sight vegetation soils.

In order to find a polarimetric parameter which is sensitivity to soil moisture, the  $\alpha_1$  from the first eigenvector is derived as

$$\alpha_1 = \arctan \left( \frac{2\sigma_{HHVV} - \left( \sigma_{VVVV} - \sigma_{HHHH} + \sqrt{(\sigma_{VVVV} - \sigma_{HHHH})^2 + 4|\sigma_{HHVV}|^2} \right)}{2\sigma_{HHVV} + \left( \sigma_{VVVV} - \sigma_{HHHH} + \sqrt{(\sigma_{VVVV} - \sigma_{HHHH})^2 + 4|\sigma_{HHVV}|^2} \right)} \right) \quad (30)$$

In Allain [28], the IEM model is used to simulate the backscattering coefficients. It is found that  $\alpha_1$  tends to be invariable with respect to the radar frequency higher than 8 GHz. At such high frequency, the  $\alpha_1$  is approximated using the IEM model as

$$\lim_{\substack{f \rightarrow \text{high} \\ \text{frequency}}} \alpha_1 = \arctan \left( \frac{2f_{hh}f_{vv}^* - \left( |f_{vv}|^2 - |f_{hh}|^2 + \sqrt{\left( |f_{vv}|^2 - |f_{hh}|^2 \right)^2 + 4|f_{hh}f_{vv}^*|^2} \right)}{2f_{hh}f_{vv}^* + \left( |f_{vv}|^2 - |f_{hh}|^2 + \sqrt{\left( |f_{vv}|^2 - |f_{hh}|^2 \right)^2 + 4|f_{hh}f_{vv}^*|^2} \right)} \right) \quad (31)$$

where the  $f_{hh}$  and  $f_{vv}$  are the parameters in the IEM model. In this case, the  $\alpha_1$  is independent of surface roughness and mainly depends on the soil dielectric constant. The potential of  $\alpha_1$  for the soil moisture retrieval is investigated in Baghdadi et al. [18] using the C-band RADARSAT-2 data, indicating it is possible to discriminate two soil moisture levels or provide necessary a priori information to enhance the accuracy of soil moisture retrieval.

### 3.2.3. Hybrid decomposition

The eigen-based decomposition is more empirically used for soil moisture retrieval, as it is inherently a mathematical approach. In contrast, the model-based decomposition based on the Bragg and Fresnel scattering models is more physically used. Recently, the combination between the model-based and eigen-based decompositions results in the hyper-decomposition [1]. Firstly, the volume scattering component is removed using the model-based decomposition. Then, the remaining ground scattering is decomposed using the eigen-based decomposition. This process overcomes the requirement of assumption on the dominant surface or dihedral scattering mechanism in the ground component (in that case, we need to assume the  $\beta$  or  $\alpha$  to be constant in order to solve the undetermined equation system).

Furthermore, as the vegetation shape and structure vary with the phenological growth, the limited volume scattering model is not sufficient to capture this complex variability. Thus, the dynamic volume scattering is developed [1], which is suitable for the entire crop phenological cycle:

$$[T_v] = \frac{f_v}{2 + 2A_p^2} \begin{bmatrix} V_{11} & V_{12} & 0 \\ V_{12}^* & V_{22} & 0 \\ 0 & 0 & V_{33} \end{bmatrix} \quad (32)$$

$$V_{11} = (A_p + 1)^2$$

$$V_{12} = (A_p^2 - 1)^2 \text{sinc}(2\Delta\varphi)$$

$$V_{22} = 0.5(A_p - 1)^2(1 + \text{sinc}(4\Delta\varphi))$$

$$V_{33} = 0.5(A_p - 1)^2(1 - \text{sinc}(4\Delta\varphi))$$

The parameters  $A_p$  and  $\Delta\phi$  were used to characterize the vegetation shape and its distribution width, respectively. With the dynamic volume model and hyper-decomposition approach, the soil moisture estimation obtained an inversion rate higher than 95% and RMSE from 4.0 to 4.4 m<sup>3</sup>/m<sup>3</sup>. In addition, for the covariance matrix, a generalized volume scattering model is proposed in [29] to quantify the vegetation scattering using the cosine-square distribution. Although the formulation varies from one to another study, the main idea relies on the characterization of the vegetation shape and orientation using the minimum number of parameters.

However, the model-based polarimetric decomposition for the soil moisture retrieval is mainly valid at L-band. When it comes to C-band, the surface roughness condition is beyond the valid range of Bragg ( $ks < 0.3$ ) or X-Bragg model ( $ks < 1$ ). In order to overcome this limitation, Huang et al. [2] first proposed a C-band polarimetric decomposition for the slight vegetation condition. In their approach, the surface scattering component is simulated using the IEM model, while the volume scattering component is formulated using the first-order sine and cosine functions for the vertical and horizontal orientations. Finally, a RMSE of 6.12 m<sup>3</sup>/m<sup>3</sup> is obtained for the soil moisture retrieval using the C-band RADARSAT-2 dataset.

## 4. Radiative scattering model

The soil moisture retrieval is performed using either physical or empirical models. We introduced below the application of integral equation model (IEM) and Oh model over the bare soil and the water cloud model (WCM) over the vegetated condition.

### 4.1. IEM model

The IEM model can be used to simulate the backscattering coefficients from incidence angle  $\theta$  and soil parameters (surface roughness  $ks$ , correlation length  $kl$ , and soil moisture  $mv$ ). Two surface roughness conditions (Gaussian or exponential) are considered to compute the corresponding backscattering coefficients. Regarding the applicability of IEM model, some studies show reasonable agreements between measurements and the model [30, 31]. However, the disagreements between measurements and model predictions are frequently observed [32–36], because the IEM model backscattering behavior depends on the autocorrelation function (ACF). Furthermore, the measurement of correlation length  $l$  is difficult to be accurate enough,

since this parameter is dependent on the profiler length as well as the number of repetition in the surface roughness measurements [37, 38].

To overcome the limitations of IEM model, Baghdadi proposed in [35, 36, 39] a calibration procedure for HH, VV, and HV polarization channels, respectively. It is assumed that the disagreements between IEM model and actual datasets are due to the selection of autocorrelation function and the in situ correlation length measurements. Therefore, after fitting a large set of experiment datasets, a calibration parameter  $l_c$  is built for different polarization channels at different incidence angles in order to take the place of measured correlation length  $l$ . The calibration parameter  $l_c$  given in [40] for C-band is described with respect to RMS surface height  $s$  and incidence angle  $\theta$ :

- For HH polarization:  $l_c = 0.162 + 3.006(\sin 1.23\theta)^{-1.194}s$
- For VV polarization:  $l_c = 1.281 + 0.134(\sin 0.19\theta)^{-1.59}s$
- For HV polarization:  $l_c = 0.9157 + 1.2289(\sin 0.1543\theta)^{-0.3139}s$

By replacing the measured correlation length with this calibration parameter, the agreement between the IEM model simulation and actual radar measurement is reported to be improved [35, 40].

#### 4.2. Oh model

The Oh model is established based on theoretical scattering models [9], scatterometer measurements, and airborne polarimetric SAR datasets (in L-, C-, and X-band, respectively) under different roughness and soil moisture conditions at incidence angles ranging from 10 to 70°. This model relates the co-polarized ratio  $p = \sigma_{HH}^0/\sigma_{VV}^0$  and the cross-polarized ratio  $q = \sigma_{HV}^0/\sigma_{VH}^0$  and absolute  $\sigma_{HV}^0$  to soil parameters (including  $s$ ,  $l$ ,  $\epsilon$ ) and radar system parameters (including the wave number  $k$  and local incidence angle  $\theta$ ).

#### 4.3. Water cloud model

As a first-order radiative transfer solution, the WCM model expresses the total backscattering signals as the summation of surface and volume scattering components,  $\sigma_{total}^0 = \Gamma^2\sigma_{surface}^0 + \sigma_{volume}^0$ . The surface scattering can be modeled using the bare soil moisture model such as the previous IEM and Oh models. The vegetation two-way attenuation on the surface scattering power is modeled by  $\Gamma^2 = \exp(-2\tau/\cos\theta)$ .

The vegetation layer is assumed to be comprised of homogenous water particles with a uniform distribution, and volume scattering component can be expressed from vegetation scattering albedo and optical depth such as  $\sigma_{volume}^0 = 0.75\omega(1 - \Gamma^2)\cos\theta$ . Accounting the polarization leads to the following empirical volume power [8]:

$$\begin{aligned}\sigma_{volume}^{VV-pola} &= \sigma_{volume}^{HH-pola} = 0.74\omega \left[ 1 + 0.54\omega\tau - 0.24(\omega\tau)^2 \right] \left[ 1 - \exp(-2.12\tau/\cos\theta) \right] \cos\theta \\ \sigma_{volume}^{HV-pola} &= \omega \left[ 0.044\omega\tau - 0.018(\omega\tau)^2 + 0.006(\omega\tau)^3 \right] \left[ 1 - \exp(-11.7\tau/\cos\theta) \right] \cos\theta\end{aligned}\quad (33)$$

At the moderate or high frequency such as C- and X-bands, the dihedral scattering is negligible. However, at low frequency such as L-band, the dihedral scattering component must be accounted, which can be quantified as [8]

$$\begin{aligned}\sigma_{dihedral}^{HH-pola} &= 1.9\omega \left[ 1 + 0.9\omega\tau + 0.4(\omega\tau)^2 \right] \left[ 1 - \exp(-1.93\tau/\cos\theta) \right] \exp(-1.37\tau^{1.12}/\cos\theta) \\ &\quad \exp(-0.84(ks)^2 \cos\theta) |R_{HH}|^2 \cos\theta \\ \sigma_{dihedral}^{HV-pola} &= 0.013\omega \left[ 1 + 7.85\omega\tau + 7.9(\omega\tau)^2 \right] \left[ 1 - \exp(-9.62\tau/\cos\theta) \right] \exp(-1.02\tau^{1.38}/\cos\theta) \\ &\quad \exp(-2.9(ks)^2 \cos\theta) \left( |R_{HH}|^2 + |R_{VV}|^2 \right) 0.5 \cos\theta \\ \sigma_{dihedral}^{VV-pola} &= 0\end{aligned}\quad (34)$$

## 5. Soil and vegetation emission model

To collect sufficient emitted energy at microwave bands, satellite radiometer uses large footprint, resulting in coarse spatial resolution. Based on the measured brightness temperature, two typical models are applied for the soil moisture retrieval: L-band Microwave Emission of the Biosphere (L-MEB) and Land Parameter Retrieval Model (LPRM). The former was mainly developed for the L-band such as the SMOS mission, while the latter was mostly used at high frequency but can be also applied to L-band. All these models were based on a simple  $\tau$ - $\omega$  model for vegetation covered lands.

*Vegetation effect:* The  $\tau$ - $\omega$  model is formulated to account for the vegetation effect on the brightness temperature. It simulates the TB at polarization  $p$  ( $h$  or  $v$ ) as the incoherent summation of (i) the soil emission attenuated by the vegetation, (ii) vegetation direct upwelling microwave emission, and (iii) vegetation downwelling emissions which are reflected by the soils and attenuated by the vegetation itself:

$$TB_p = E_p \gamma_p T_{soil} + (1 - \omega) (1 - \gamma_p) T_{vege} + (1 - \omega) (1 - \gamma_p) T_{vege} R_p \gamma_p \quad (35)$$

where  $T_{soil}$  and  $T_{vege}$  are soil and vegetation effective temperatures, respectively. The soil emissivity  $E_p = (1 - R_p)$  is computed from the soil reflectivity ( $R_p$ ). The vegetation attenuation on the soil emission is modeled through a vegetation transmissivity  $\gamma_p$  which is a function of the optical depth  $\tau_p$  and incidence angle  $\theta$ :

$$\gamma_p = e^{-\tau_p/\cos(\theta)} \quad \text{and} \quad \tau_p = b_p \cdot VWC \quad (36)$$

At L-band, the vegetation scattering albedo  $\omega$  is assumed to be close to zero and independent of the polarization and incidence angle [41].

*Surface roughness effect:* assuming the surface scattering over the interface between soil and air, the rough soil reflectivity  $R_p$  was obtained from the smooth surface reflectivity  $r_p$ :

$$R_p = [(1 - Q) \cdot r_p + Q \cdot r_q] \cdot \exp(-H_r \cos^{N_p}(\theta)) \quad (37)$$

where  $r_p$  is the Fresnel coefficients for h and v polarizations:

$$r_h = \left| \frac{\cos \theta - \sqrt{\epsilon_s - \sin^2 \theta}}{\cos \theta + \sqrt{\epsilon_s - \sin^2 \theta}} \right|^2 \quad (38)$$

$$r_v = \left| \frac{\epsilon_s \cos \theta - \sqrt{\epsilon_s - \sin^2 \theta}}{\epsilon_s \cos \theta + \sqrt{\epsilon_s - \sin^2 \theta}} \right|^2$$

The parameter  $Q$  quantifies the polarization mixing degree due to the surface roughness and is neglected at L-band [42, 43].  $N_p$  represents the dependence of roughness on incidence angle. Furthermore, the effective surface roughness parameter  $H_r$  is associated to the measured surface roughness in a conventional way:

$$H_r = 4k^2 s^2 \quad (39)$$

with wave number  $k$  and surface *RMS* height  $s$ . However, the clear general relationship between  $H_r$  and measured surface roughness is still uncertain. In the literature, different empirical relationships were established to link the  $H_r$  parameter to surface *RMS* height and the autocorrelation length [44]. The  $H_r$  parameter is also found to be influenced by soil moisture, but it is reported to be mainly valid for the sandy soils [42].

## 6. Joint active-passive microwave for soil moisture estimation

The radar signal comprised of the amplitude and phase is coherent and more influenced by the surface roughness and vegetation. In contrast, the radiometer signal is incoherent, reducing the influences from the surface roughness and vegetation. In addition, the radar signal is acquired with high spatial resolution at the cost of narrow swath range, while the radiometer signal has a frequent revisit cycle but coarse spatial resolution. In order to combine the advantages of the radar and radiometer signals, recent studies go into the soil moisture retrieval by a joint active-passive approach. In this context, the original objective of the SMAP mission is to monitor the soil moisture by the active-passive combination, although the radar component failed.

For the airborne platform, the active and passive signals can be obtained with a similar spatial resolution. The optimization process is conducted to match the microwave signals to the

model output. For instance, the following cost function was constructed [45] by using both the radar and radiometer signals:

$$C(X) = 0.5 \left[ \sum \left| \frac{\sigma_{pq}^{data} - \sigma_{pq}^{simu}(X)}{\sigma_{pq}^{data}} \right|^2 + \gamma \cdot \sum \left| \frac{TB_p^{data} - TB_p^{simu}(X)}{TB_p^{data}} \right|^2 \right] \quad (40)$$

where  $\sigma_{pq}^{data}$  and  $TB_p^{data}$  are the real data from the radar and radiometer, respectively.  $\sigma_{pq}^{simu}(X)$  and  $TB_p^{simu}(X)$  are the simulated radar and radiometer signals. The  $\gamma$  is a tuning parameter to balance the radar and radiometer signals in the optimization process. The increase of  $\gamma$  represents the enhanced contribution of the radiometer signals for the soil moisture retrieval. The airborne Passive-Active L-band Sensor (PALS) data were collected during the SMAPVEX12 and SMAPVEX16 campaigns, providing an opportunity to develop the active-passive soil moisture retrieval approaches.

For the spaceborne platform, such as the condition of the original SMAP mission, the radar and radiometer signals have different spatial resolutions. In this case, the radar signal with fine spatial resolution is used to disaggregate the radiometer signal with coarse resolution to obtain TB data with moderate resolution, considering the correlation between the radar and radiometer signals. Then, the emission model was applied to the disaggregated brightness temperature to retrieve the soil moisture at a moderate spatial resolution.

## Author details

Hongquan Wang<sup>1,2\*</sup>

\*Address all correspondence to: hongquan.wang@usherbrooke.ca

1 College of Environmental and Resource Sciences, Zhejiang University, Hangzhou, China

2 CARTEL, University of Sherbrooke, Sherbrooke, QC, Canada

## References

- [1] Jagdhuber T, Hajnsek I, Papathanassiou KP. An iterative generalized hybrid decomposition for soil moisture retrieval under vegetation cover using fully polarimetric SAR. *IEEE Journal of Selected Topics in Applied Earth Observations and Remote Sensing*. 2015;8(8): 3911-3922
- [2] Huang X, Wang J, Shang J. An integrated surface parameter inversion scheme over agricultural fields at early growing stages by means of C-Band polarimetric RADARSAT-2 imagery. *IEEE Transactions on Geoscience and Remote Sensing*. 2016;54(5):2510-2528

- [3] Baver LD, Gardner WH, Gardner WR. Soil Physics. New York: Wiley; 1977
- [4] Topp GC. Electromagnetic determination of soil water content: Measurements in coaxial transmission lines. *Water Resource Research*. 1980;**16**(3):574-582
- [5] Hallikainen MT, Ulaby FT, Dobson MC, et al. Microwave dielectric behavior of wet soil-part 1: Empirical models and experimental observations. In: *IEEE Transactions on Geoscience and Remote Sensing*. Vol. 23; 1985. pp. 25-34
- [6] Toogood JA. A simplified textural classification diagram. *Canadian Journal of Soil Science*. 1958;**38**:54-55
- [7] Rowell DL. *Soil Science: Methods and Applications*. Harlow, UK: Longman Scientific & Technical; 1994
- [8] Ulaby FT, Moore RK, Fung AK. *Microwave Remote Sensing: Active and Passive, Vol. III – Volume Scattering and Emission Theory, Advanced Systems and Applications*. Norwood, USA: Artech House; 1986
- [9] Ulaby FT, Moore RK, Fung AK. *Microwave Remote Sensing: Active and Passive, Vol. II – Radar Remote Sensing and Surface Scattering and Emission Theory*. Norwood, US: Addison-Wesley Publishing Company, Advanced Book Program/World Science Division; 1982
- [10] Daniel S. *Analysis d'images SAR polarimetriques aeroportees pour l'estimation de parametres bio-physiques des sols agricoles*. Universite de Rennes 1; 2009
- [11] Dobson MC, Ulaby FT, Hallikainen MT, et al. Microwave dielectric behavior of wet soil-part II: Dielectric mixing models. *IEEE Transactions on Geoscience and Remote Sensing*. 1985;**GE-23**:35-46
- [12] Mironov VL, Kosolapova LG, Fomin SV. Physically and mineralogically based spectroscopic dielectric model for moist soils. *IEEE Transactions on Geoscience and Remote Sensing*. 2009;**47**(7):2059-2070
- [13] Mandelbrot BB. *The Fractal Geometry of Nature*. San Francisco, CA: Freeman; 1982
- [14] Falconer K. *Fractal Geometry, Mathematical Foundations and Applications*. New York: John Wiley and Sons; 1990
- [15] Zribi M, Ciarletti V, Taconet O, et al. Characterisation of the soil structure and microwave backscattering based on numerical three-dimensional surface representation: Analysis with a fractional Brownian model. *Remote Sensing of Environment*. 2000;**72**:159-169
- [16] Jaynes ET. *Probability Theory: The Logic of Science*. Cambridge, UK: Cambridge University Press; 2003
- [17] Hajnsek I. *Inversion of Surface Parameters using Polarimetric SAR*. Jena, Germany: Friedrich-Schiller-Universitat Jena; 2001
- [18] Baghdadi N, Cresson R, Pottier E, et al. A potential use for the C-band polarimetric SAR parameters to characterize the soil surface over bare agriculture fields. *IEEE Transaction on Geoscience and Remote Sensing*. 2012;**50**(10):3844-3858

- [19] Hajnsek I, Jagdhuber T, Schon H, et al. Potential of estimating soil moisture under vegetation cover by means of PolSAR. *IEEE Transaction on Geoscience and Remote Sensing*. 2009;**47**(2):442-454
- [20] Jagdhuber T, Hajnsek I, Bronstert A, et al. Soil moisture estimation under low vegetation cover using a multi-angular polarimetric decomposition. *IEEE Transaction on Geoscience and Remote Sensing*. 2013;**51**(4):2201-2215
- [21] Wang H, Magagi R, Goita K, et al. Evaluation of simplified polarimetric decomposition for soil moisture retrieval over vegetated agricultural fields. *Remote Sensing*. 2016; **8**(2):142
- [22] Yamaguchi Y, Moriyama T, Ishido M, et al. Four-component scattering model for polarimetric SAR image decomposition. *IEEE Transaction on Geoscience and Remote Sensing*. 2005;**43**(8):1699-1706
- [23] Freeman A, Durden SL. A three-component scattering model for polarimetric SAR data. *IEEE Transaction on Geoscience and Remote Sensing*. 1998;**36**(3):963-973
- [24] An W, Cui Y, Yang J. Three-component model-based decomposition for polarimetric SAR data. *IEEE Transaction of Geoscience and Remote Sensing*. 2010;**48**(6):2732-2739
- [25] Wang H, Magagi R, Goita K. Comparison of different polarimetric decompositions for soil moisture retrieval over vegetation covered agricultural area. *Remote Sensing of Environment*. 2017;**199**(1):120-136
- [26] Jagdhuber T. An approach to extended Fresnel scattering for modeling of depolarizing soil-trunk double-bounce scattering. *Remote Sensing*. 2016;**8**(10). Article No. 818
- [27] Hajnsek I, Pottier E, Cloude SR. Inversion of surface parameters from polarimetric SAR. *IEEE Transactions on Geoscience and Remote Sensing*. 2003;**41**(4):727-744
- [28] Allain S. Caractérisation d'un sol nu à partir de données SAR polarimétriques étude multi-fréquentielle et multi-résolutions. Université de Rennes 1; 2003
- [29] Arii M, vanZyl JJ, Kim Y. Adaptive model-based decomposition of polarimetric SAR covariance matrices. *IEEE Transactions on Geoscience and Remote Sensing*. 2011;**49**(3): 1104-1113
- [30] Shi JC, Wang J, Hsu AY, et al. Estimation of bare surface soil moisture and surface roughness parameter using L-band SAR image data. *IEEE Transaction on Geoscience and Remote Sensing*. 1997;**35**(5):1254-1266
- [31] Bindlish R, Barros AP. Multifrequency soil moisture inversion from SAR measurements with the use of IEM. *Remote Sensing of Environment*. 2000;**71**:67-88
- [32] Mattia F, Le Toan T, Souyrb J, et al. The effect of surface roughness on multifrequency polarimetric SAR data. *IEEE Transactions on Geoscience and Remote Sensing*. 1997;**35**: 954-966
- [33] Zribi M, Taconet O, Hégarat-Masclé SL, et al. Backscattering behavior and simulation comparison over bare soils using SIR-C/X-SAR and ERASME 1994 data over Orgeval. *Remote Sensing of Environment*. 1997;**59**:256-266

- [34] Baghdadi N, Gherboudj I, Zribi M, et al. Semi-empirical calibration of the IEM backscattering model using radar images and moisture and roughness field measurements. *International Journal of Remote Sensing*. 2004;**25**:3593-3623
- [35] Baghdadi N, Holah N, Zribi M. Calibration of the integral equation model for SAR data in C-band and HH and VV polarizations. *International Journal of Remote Sensing*. 2006;**27**:4
- [36] Baghdadi N, Chaaya JA, Zribi M. Semi-empirical calibration of the integral equation model for SAR Data in C-band and cross polarization using radar images and field measurements. *IEEE Geoscience and Remote Sensing Letters*. 2011;**8**(1):14-18
- [37] Altese E, Bolognani O, Mancini M, et al. Retrieving soil moisture over bare soil from ERS-1 synthetic aperture radar data: Sensitivity analysis based on a theoretical surface scattering model and field data. *Water Resources Research*. 1996;**32**:653-661
- [38] Oh Y, Kay YC. Condition for precise measurement of soil surface roughness. *IEEE Transactions on Geoscience and Remote Sensing*. 1998;**36**(2):691-695
- [39] Baghdadi N, King C, Bonnifait L. An empirical calibration of the Integral Equation Model based on SAR data and soil parameters measurements. *IEEE International Geoscience and Remote Sensing Symposium*. Toronto, Canada. June 24-28 2002
- [40] Dong L, Baghdadi N, Lu R. Validation of the AIEM through correlation length parameterization at field scale using radar imagery in a semi-arid environment. *IEEE Geoscience and Remote Sensing Letters*. 2013;**10**:461-465
- [41] Wigneron JP, Parde M, Waldteufel P, et al. Characterizing the dependence of vegetation model parameters on crop structure, incidence angle, and polarization at L-band. *IEEE Transactions on Geoscience and Remote Sensing*. Feb. 2004;**42**(2):416-425
- [42] Martens B, Lievens H, Colliander A, et al. Estimating effective roughness parameters of the L-MEB Model for soil moisture retrieval using passive microwave observations from SMAPVEX12. *IEEE Transactions on Geoscience and Remote Sensing*. 2015;**53**(7):4091-4103
- [43] Wang JR, Neill PEO, Jackson TJ, et al. Multifrequency measurements of the effects of soil moisture, soil texture, and surface roughness. *IEEE Transactions on Geoscience and Remote Sensing*. 1983;**GE-21**(1):44-51
- [44] Lawrence H, Wigneron JP, Demontoux F, et al. Evaluating the semiempirical H-Q model used to calculate the L-Band emissivity of a rough bare soil. *IEEE Transactions on Geoscience and Remote Sensing*. 2013;**51**(7):4075-4084
- [45] Akbar R, Moghaddam M. A combined active-passive soil moisture estimation algorithm with adaptive regularization in support of SMAP. *IEEE Transactions on Geoscience and Remote Sensing*. 2015;**53**(6):3312-3324